Nuclear Materials and Energy 24 (2020) 100780

Contents lists available at ScienceDirect

Nuclear Materials and Energy

journal homepage: www.elsevier.com/locate/nme

Influence of 1 and 5 wt% TiC additions on the oxidation behaviour of pure tungsten

Pablo Pérez[a], Miguel A. Monge[b,*], Ángel Muñoz[b], Paloma Adeva[a]

[a] Centro Nacional de Investigaciones Metalúrgicas (CENIM-CSIC), Departamento de Metalurgia Física, Avd. Gregorio del Amo 8, 28040 Madrid, Spain
[b] Universidad Carlos III de Madrid, Dpto. de Física, Avda. de la Universidad 30, Leganés 28911, Spain

ARTICLE INFO

Keywords:
Tungsten
Composites
Oxidation resistance
Reinforced materials
TiC
Titanium carbide

ABSTRACT

The influence of 1 and 5 wt% of TiC nanoparticles on the oxidation behaviour of reinforced tungsten has been evaluated up to 700 °C in dry air. Isothermal thermogravimetric tests prove that the addition of 5 wt% of TiC particles is detrimental, increasing the mass gain of pure tungsten by a factor of ten. TiC particles act as stress concentrators, facilitating microcracking events within the scale and promoting decohesion between TiC-free boundaries and TiC-containing regions of the material. Compared to pure tungsten, lowering TiC addition to 1 wt% significantly improves the oxidation resistance at 700 °C by reducing about seven times the mass gain, while at 600 °C both materials exhibit similar resistance. At 700 °C, the presence of 1 wt% of TiC particles inhibits massive microcracking events occurring in the scale formed on pure tungsten, rendering the oxide scale denser and more protective.

1. Introduction

The major technical decision concerning the change to a full-tungsten divertor for ITER (International Thermonuclear Experimental Reactor), instead of the initial carbon fibre monoblocks design due to the risk of rapid accumulation of tritium by codeposition [1,2], was the last approved by IO (ITER Organization) in the selection of materials for a critical component of the first wall of the reactor vessel after a successful two-year qualification program of intensive research [3-5]. Tungsten was the only material industrially available with well-established properties and manufacturing technologies that fulfilled the stringent technical and operative requirements of the divertor. This is due to the unique properties of tungsten for sustaining extreme temperature working conditions, high thermal loads, heavy erosion from very energetic particles, and a high resistance for irradiation with a low retention of tritium and an acceptable activation and transmutation behaviour under the 14 MeV fusion neutron [6].

These properties have made tungsten and tungsten-based materials the main candidate materials for Plasma Facing Components (PFCs) of future fusion reactors such as DEMO [7]. However, pure tungsten has a high ductile to brittle temperature transition that increases under neutron irradiation, a tendency to self-castellation that have been observed in tungsten monoblocks after extreme thermal loads, and a poor oxidation resistance that can lead to the formation of volatile oxides. This last property generates a serious security risk issue in case of a loss of coolant accident (LOCA) followed by a vacuum integrity loss of the reactor vessel (LOVA) [8]. An emergency shutdown of the reactor in this accidental scenario will rise the temperature of the PFCs up to ~ 1200 °C for a period longer than ten days due to nuclear decay heat, resulting in a fast oxidation of pure tungsten components, formation of volatile oxides, with sublimation rates of 10–100 kg h^{-1} for a full-tungsten divertor, and release of a radioactive cloud to the environment [8].

DEMO and future commercial reactors will require higher performance materials than pure W, with superior mechanical properties, thermal resistance and radiation resistance [6,7]. As example, radiation damage of PFCs in DEMO is of about 150 dpa [9] after five years of full power operation compared to ~ 3 dpa for ITER. Tungsten alloys and composites such as WTi, WCrTi, WCrY or WKY have been proposed for structural applications and PFCs, but the lower melting point of the alloying elements results in a reduction of the upper working temperature [10-13]. Tungsten reinforced with a fine dispersion of titanium carbide (TiC) particles, with a melting point of 3067 °C, has an increased resistance to neutron irradiation and enhanced ductility from room temperature up to high working temperatures that reduces the embrittlement that pure W exhibits at different temperature regimes [14,15]. This makes W-TiC composites a promising material for PFCs.

In the last years, a significant effort has been developed to study the

* Corresponding author.
E-mail address: mmonge@fis.uc3m.es (M.A. Monge).

https://doi.org/10.1016/j.nme.2020.100780
Received 31 January 2020; Received in revised form 14 July 2020; Accepted 17 July 2020
Available online 23 July 2020

oxidation mechanism and resistance of materials with potential application in PFCs to stablish the safety of the reactor in case of plausible accidental scenarios [16,17]. However, the oxidation resistance of W-TiC composites has not been studied to our knowledge to ensure in service safety in case of a LOCA and/or LOVA accidents.

In the present study, the oxidation behaviour in dry air of tungsten reinforced with a dispersion of 1 and 5 wt% of TiC nanoparticles produced by mechanical alloying and high isostatic pressing has been evaluated. Isothermal thermogravimetric measurements in air at different temperatures were performed on samples with TiC contents up to 5 wt%, and the oxide scales were characterized by X-Ray diffraction and SEM microscopy to stablish the oxidation resistance and the mechanisms controlling the oxidation process.

2. Materials and methods

Two TiC particle-reinforced tungsten ingots with compositions W-1wt.%TiC (designated as W-1TiC) and W-5wt.%TiC (designated as W-5TiC) were prepared from starting powders of elemental W and TiC particles, having a purity and average particle size of 99.95% and 1–5 μm for W, and 99.5% and ≈5 nm for TiC, respectively. The powders were blended for 4 h in a Turbular T2F mixer, mechanical alloyed in a high-energy planetary ball mill at 150 r.p.m. for 50 h with tungsten carbon balls of 10 mm in diameter as grinding media, and finally sintered by hot isostatic pressing at 1573 K for 2 h after encapsulation and degassing. All the production processes were performed under a high purity argon atmosphere and they have been already presented elsewhere [11].

After surface polishing, the microstructure of the samples was studied with a high-resolution scanning microscope (SEM) FE-SEM FEI TENEO, equipped with an energy dispersive X-Ray spectroscopy (EDAX) detector.

Oxidation tests at 600 and 700 °C in dry air were carried out on coupons of 10 × 10 × 1 mm^3. All major surfaces were abraded on successively finer papers, mechanically polished with a 0.3 μm alumina suspension and cleaned with ethanol. Mass gain curves were continuously recorded during isothermal thermogravimetric tests for exposures up to 100 h. A continuous flow of dry air (dewpoint below − 40 °C) was supplied using an air compressor.

The characterization of the oxidation products was performed on samples used for mass gain determination and on samples isothermally oxidized for short oxidation times to analyse the evolution of the oxide scale in the initial oxidation stages. Phase identification of the oxides constituting the oxide scale was performed by X-ray diffraction (XRD) using Co-Kα radiation. The microstructure of the surfaces and cross-sections of the oxidized specimens were studied by scanning electron microscopy (SEM). For preventing discharges during SEM observations, the oxide scale was sputtered with a thin conductive gold film. After the characterization of the outer surface of the oxide scales, a thick copper coating was deposited over the gold layer to avoid damaging the oxide scale during the metallographic preparation of cross sections of oxidized samples. The composition of the oxides was qualitatively analysed by energy dispersive X-ray microanalysis (EDX).

3. Results

The initial characterization of the microstructure of the as-HIPed composites and the study of their mechanical properties from room temperature up to 1200 °C were already reported elsewhere [11]. Fig. 1 shows the fine microstructure of W-1TiC and W-5TiC materials. The tungsten matrix of W-1TiC is characterized by equiaxed recrystallized grains with an average grain size of (310 ± 30) nm and the presence of two types of precipitates: i) irregular coarse-shaped particles located at the grain boundaries with sizes up to 0.8 μm, and ii) small rounded precipitates, some inside the W matrix, with sizes ranging from 18 to 40 nm (see Fig. 1a and 1b) [11]. The exhaustive analysis of numerous EDS spectra of both types of precipitates demonstrates that they correspond to TiC particles. Fig. 1 (e)-(f) depicts the elemental distribution of W and Ti on the W-1TiC and W-5TiC composites (EDS scanning measurements with a beam energy of 25 kV), showing that Ti is found on coarse particles at the grain boundaries, and inside the tungsten grains as small TiC precipitates. The reinforcing TiC particles are larger than the initial ones of the TiC powders, indicating that coarsening or re-precipitation processes are responsible for their formation, since coalescence of the initial TiC was not observed on the milled powders [11]. The density and size of coarse precipitates located at grain boundaries increase with the TiC content (see Fig. 1). W-5TiC exhibits a similar microstructure but with two important major differences. Firstly, the W matrix consists of ultra-fine grains with an estimated average size of (130 ± 30) nm, although some coarse recrystallized tungsten grains, up to 0.85 μm, were also noticed. The second difference is the presence of a larger density of coarse TiC particles at the grain boundaries.

Mass gain curves of W-1TiC alloy at 600 °C and 700 °C, and W-5TiC at 600 °C are presented in Fig. 2. Test at 700 °C for the W-5TiC was not possible because of its enormous mass gain increase at this temperature. For comparison purposes, mass gain curves of pure tungsten processed by conventional and powder metallurgy routes are also depicted in Fig. 2. At 600 °C, mass gain curves show that an increase in the weight fraction of TiC particles considerably affects the oxidation resistance of pure tungsten. The mass gain of the W-1TiC material after 100 h of oxidation is about nine times lower than that presented by W-5TiC, 8 and 138 mg/cm^2, respectively. Moreover, W-1TiC exhibited a slightly lower mass gain than pure tungsten (ITER grade) produced through a conventional processing route (8 and 11 mg/cm^2, respectively) but it is somewhat higher than the exhibited by pure tungsten processed following the same powder metallurgy route of the studied W-TiC materials. The kinetics of the oxidation process were calculated by adjusting the experimental curves to a power law of the form $\Delta W = kt^n$, where ΔW is the mass gain per unit area, k the oxidation rate constant, n the oxidation rate exponent, and t the exposure time. Results evidence changes in the n exponent as the oxidation progresses, as presented in Fig. 2c. In the case of the W-1TiC, the kinetics are governed by parabolic laws ($n \approx 0.5$) during the first 10 h of oxidation. For longer exposure times, the kinetics changes from parabolic to linear $n \approx 1$. On the other hand, W-5TiC material exhibits linear kinetics from the initial stages of oxidation over the entire exposure. The results evidence significant differences on the oxidation behaviour between W-1TiC/W-5TiC materials from that reported for pure tungsten [17]. The oxidation kinetics of pure tungsten obey a parabolic law at 600 °C, interrupted by short periods where the kinetics turn linear until a new parabolic regime is again reached. Change from parabolic to linear kinetics is caused by accumulation of growth stresses which are released through local cracking events in the oxide scale [17]. At 700 °C, the mass gain curve of W-1TiC exhibits much lower values than those reported for pure tungsten, disregarding the processing route. This explains the lower mass gain of W-1TiC, 22 mg/cm^2, which is about seven times lower than that reported for pure tungsten [17]. The oxidation proceeds following a parabolic kinetics during the first 30 h of oxidation, changing to linear afterwards (see Fig. 2c). However, the mass gain tends to decrease after this breakaway period, although kinetics does not return to a parabolic law. Pure tungsten has a totally different behaviour, which is characterized by linear kinetics from the initial stages of oxidation [16,17].

The evolution of the morphology of the scale was studied after short- and long-term periods of oxidation. Fig. 3 presents the surface of the W-1TiC material after 7 h of oxidation at 600 °C. At low magnifications, a homogeneous cracked oxide film is observed on the surface of the alloy, being the cracks generated during cooling down from the furnace (see Fig. 3a). SEM images reveal a relatively dense scale spotted sporadically by nodules/particles in which the oxide can appear with different morphologies, as coarse blocks or rosettes made of long laths

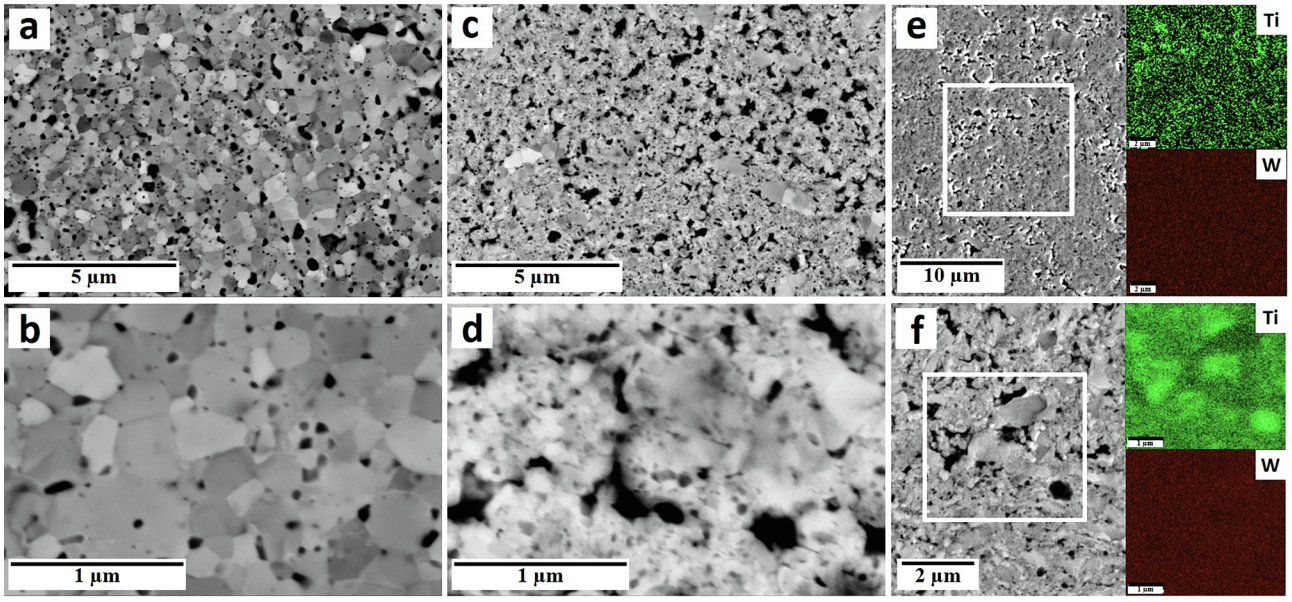

Fig. 1. SEM-BSE images of (a-b) Ti-1TiC and (c-d) Ti-5TiC showing a matrix of submicrometric tungsten grains (gray contrast) decorated with TiC particles (black contrast) at the grain boundaries and inside the grains. Figures (e) and (f) correspond to EDS mappings depicting the elemental distribution of Ti and W on W-1TiC and W-5TiC composites, respectively.

growing outside the scale, and the presence of some isolated pores (see inset of Fig. 3a). Higher-magnification SEM images prove that the oxide scale is composed of fine crystals of about 200–300 nm in size (Fig. 3b). Analysis of the measured X-ray patterns revealed that the scale consists of a mixture of WO_3, $W_{18}O_{49}$ and $WO_{2,92}$ oxides (Fig. 4a). After 100 h of exposure, the scale becomes apparently denser (see Fig. 4b), made of larger crystals of about 300 to 600 nm (see inset on Fig. 4b). The surface of the scale is sprinkled by numerous block shaped coarse particles of about 2–5 µm, nodules of about 10 µm in diameter and craters of about 15 µm in size, as observed in Fig. 4b. Due to the higher mass gain of the W-5TiC, the surface was examined after 1 h of oxidation to study the initial stages of the oxide scale formation. At this early stage, Fig. 4c reveals a smooth layer consisting of fine oxide grains of about 50–100 nm, with some coarse nodules randomly dispersed, and numerous shallow grooves/cavities (see inset of Fig. 4c). The morphology of the scale after 100 h is similar to that developed after 1 h of exposure, with a crystal size in the same range, 50–100 nm (see inset of Fig. 4d), although the grooves/cavities become deeper and the flat aspect of the surface turns to be convoluted (Fig. 4d). The morphology of the surface scale on the W-1TiC material after 100 h of exposure at 700 °C resembles that of the sample tested 100 h at 600 °C. The major differences arise from the large number of craters present on the surface (Fig. 4e) and the fact that the external scale is overgrown by large number of particles, generally prismatic rods growing outwards and perpendicularly to the scale (Fig. 4f). The nature of these particles is the same as those observed in craters, but the size of the prismatic rods is higher on crater walls (see inset of Fig. 4f)

Fig. 5a presents the cross-sectional views of the oxide scale formed on the W-1TiC after 7 h of oxidation at 600 °C. The thickness of the scale was rather uniform, about 7–7.5 µm, but the oxide/substrate interface presents a wavy aspect. The outermost part of the scale is very dense and practically free of porosity while the innermost part contains abundant porosity and some large cavities. It is interesting to note that cavity formation seems to develop at the same depth, 3 µm from the air/scale interface, in the central part of the oxide scale. Coarse TiC particles remain embedded within the oxide scale and they seem to be associated with the formation of long thin cavities oriented along the growth direction (see inset of Fig. 5a). The thickness of the scale increases as the oxidation process proceeds, up to about 70 µm after 100 h at 600 °C (Fig. 5b). The scale alternates layers of relatively dense regions with other less compact regions which contain semicontinuous arrangements of cavities running parallel to the original surface (indicated by arrows in the inset of Fig. 5b). The thickness of the individual layers remains similar along the whole cross section, indicative of a growth mechanism which is periodically repeated in the course of the oxidation process. The W-5TiC develops a rather thick oxide layer, of about 21 µm, after 1 h of exposure at 600 °C, as expected from the considerable mass gain measured for this material (see Fig. 5c). High-magnification SEM images reveal profuse cavity formation. Two types of cavities can be distinguished; (i) thin discontinuous cavities running parallel to the original exposed surface, forming small layered substructures that appear every 0.5–1 µm, as marked by red lines on Fig. 5c. (ii) Thick cavities running in the oxide growth direction. These cavities become several microns long and they are bordering dense oxide regions present in the scale (marked with blue arrows on Fig. 5c. This pattern is repeated across the entire thickness of the scale when the material is further exposed up to 100 h, indicating that a unique oxidation mechanism is operating during the entire oxidation process (see Fig. 6). The thickness of the scale after 100 h of oxidation is rather thick, 1.5 mm. After 100 h of exposure at 700 °C, W-1TiC formed a thick scale of about 144 µm, as depicted on the cross section of Fig. 5d. The structure of the oxide is quite different to that developed on the material tested at 600 °C. It consists of a porous layer with the cavities oriented in the oxide growth direction, without the arrangements of cavities parallel to the original surface observed after exposure at 600 °C.

4. Discussion

The present study proves that the influence of TiC on the oxidation behaviour of pure tungsten depends on the content of TiC particles and the temperature. The presence of coarse TiC particles controls the oxidation resistance. A high content of coarse TiC particles, as in the case of W-5TiC, promotes linear kinetics from the initial stages of oxidation which leads to accelerated oxidation. Consequently, the oxidation of W-5TiC proceeds at 600 °C at least ten times faster than for pure tungsten. However, when the TiC content is reduced to 1 wt%, the oxidation behaviour experiences significant changes. The mass gain

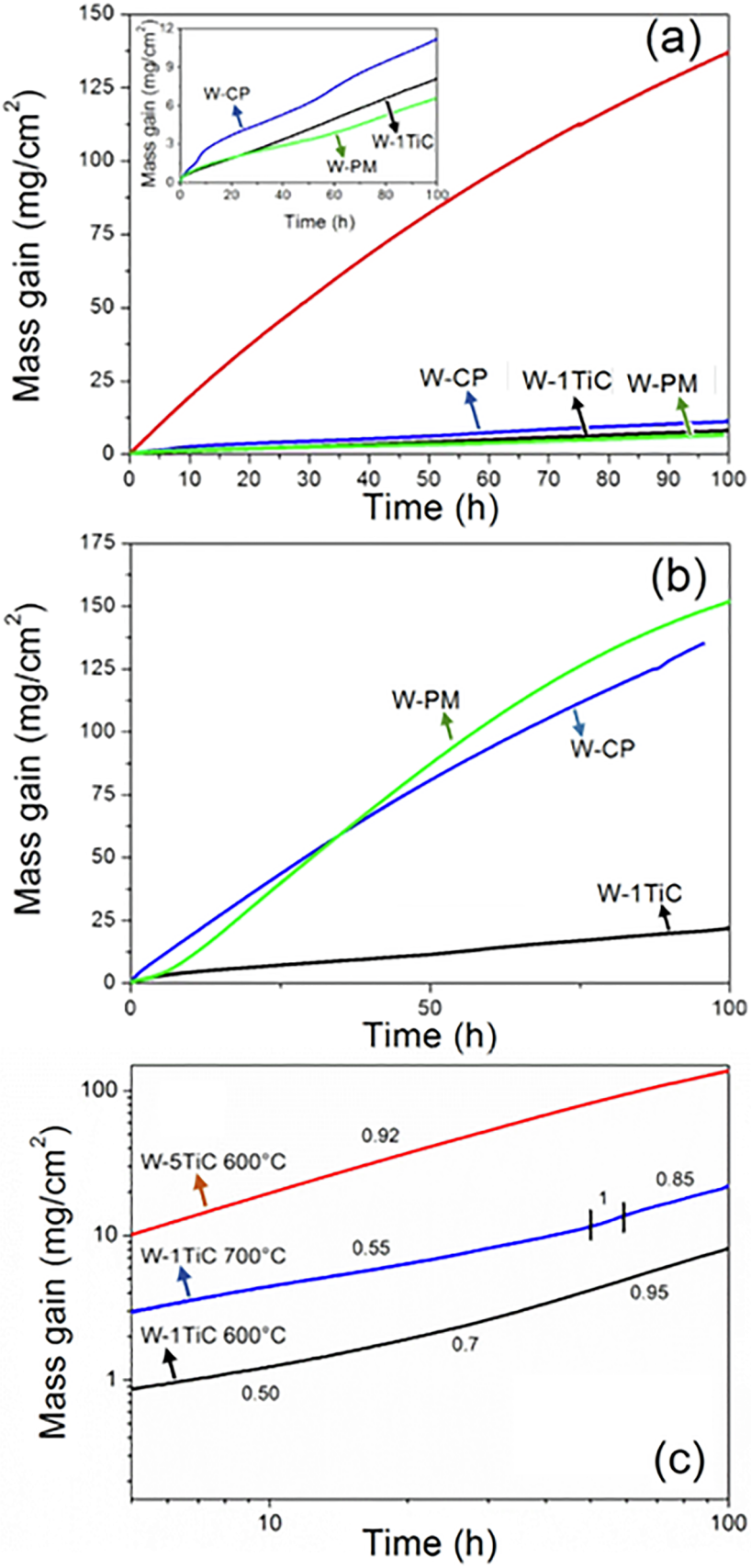

Fig. 2. Mass gain curves for oxidation tests in dry air for W-1TiC and W-5TiC materials (curves corresponding to pure tungsten processed by a conventional route (W-CP) and a powdermetallurgy route (W-PM) are also depicted with a comparative purpose). (a) Tested at 600 °C. The inset presents the curves for W-1TiC, W-CP and W-PM. (b) Tested at 700 °C. (c) Double logarithmic plot of the oxidation kinetics curves.

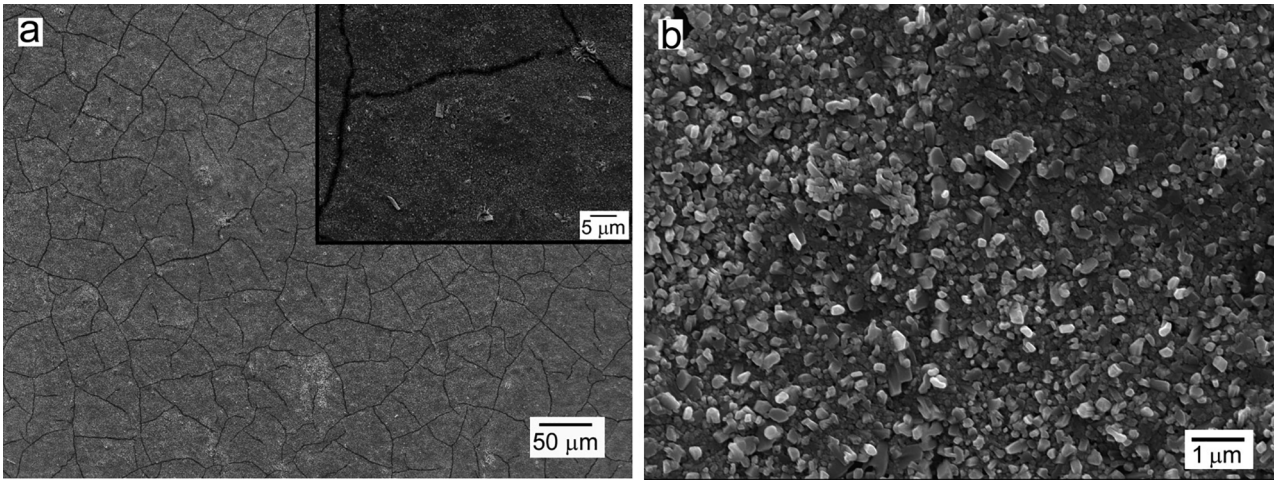

Fig. 3. (a) Surface image of the scale formed on the W-1TiC material after 7 h of exposure in dry air at 600 ˚C. The inset is a detail of the oxidized surface at higher magnifications. (b) Detail of the oxide morphology.

measured for W-1TiC at 600 ˚C is similar to the values reported for pure tungsten. Nevertheless, the kinetics is considerably slowed down at 700 ˚C, with mass gains decreasing by a factor of seven compared to pure tungsten.

It is necessary to understand how the change in the volume fraction of TiC particles influences drastically the oxidation performance of tungsten, especially considering that TiC addition does not affect significantly to the composition of the oxide scale, which is composed of tungsten oxides. According to EDX microanalyses, TiC particles seems to be linked with cavity formation due to the detection of Ti, C, W and O peaks in the spectra measured in the particles located at cavities (see Fig. 7). The low intensity of the carbon peak indicates that TiC particles are probably oxidized as rutile, as reported during oxidation for other alloys reinforced by TiC phase [18,19]. Nevertheless, no rutile peaks were indentified in the XRD patterns, so it cannot be ruled out the formation of W-Ti-O oxides, as could be expected from the large intensity of W and O peaks in the EDX spectra. Although no peaks could be unequivocally attributed to (W,Ti)-rich oxides in XRD pattern, some of the small peaks non-identified in XRD patterns could correspond to this oxide. Moreover, the decrease in the intensity of C peak as the oxidation proceeds indicates that the entire TiC particles will become oxidized after long-term exposures.

The structure of the scales provides relevant information about the possible reasons of the different behaviour of W-TiC materials depending on their TiC content. In the case of the W-1TiC the relatively dense protective scale formed from the initial stages of oxidation accounts for the parabolic kinetics. After this initial stage, the presence of periodical arrangements of discontinuous cavities is observed throughout the thickness of the scale. This change from a dense scale to a multi-layered scale is accompanied with a change from parabolic to linear kinetics. In the case of the W-5TiC, the tendency for the formation of cavities is substantially increased. Therefore TiC particles act in a double way. Firstly, TiC particles promote cavity formation. The cavities act as stress concentrators, increasing locally the growth stresses of the oxide and favouring microcracking events within the scale. Secondly, TiC particles interrupt the continuity of tungsten oxides, favouring decohesion between TiC-free boundaries and TiC-containing regions. Coarse TiC particles are mostly located at grain boundaries and the stresses induced by the large change in volume associated with oxide formation separate both regions, resulting in the development of long perpendicular cracks. These perpendicular cracks are suppressed when the amount of TiC coarse particles is decreased, as in the case of the W-1TiC, where cracking is restricted to very few regions, leading to a more protective oxide scale which resembles that reported for pure tungsten [17,20]. On the other hand, massive cracking in the W-5TiC favours rapid oxygen ingress and rapid oxidation of the material.

The oxidation mechanism in W-1TiC is very similar to that reported for pure tungsten. Protection is conferred by the formation of a protective $W_{18}O_{49}$ layer [17], as this phase was equally found in XRD patterns of the W-1TiC material oxidized for 7 h at 600 ˚C (see Fig. 4a). Growth stresses, however, induce local microcracking of this layer in multiple points, promoting rapid ingress of oxygen into the substrate. This microcracking is accompanied by the development of cavities according to the model proposed by Cifuentes and co-workers [17]. Oxygen transport through microcracks is momentarily delayed compared to oxygen transport in neighboured non-cracked regions. As consequence, new oxide is rapidly formed and the large volume increase associated with its formation moves the scale outwards, resulting in the formation of cavities until oxygen transport in the cavity permits the formation of the oxide at the bottom of cavities. At this moment, the scale continues to form as a compact layer until a new event of massive local cracking takes place. Since EDX of cavities in W-1TiC reveals the presence of Ti and C, i.e. of non-totally oxidized TiC coarse particles, the effect of TiC particles is similar to that due to the microcracks. When the oxidation front reaches coarse TiC particles, they are not immediately oxidized, constituting a transitory barrier for oxygen ingress. Consequently, the oxidation front should surround such particles during its inward growth and the enormous stresses associated with oxide formation drag TiC particles outwards, leading to the formation of cavities whose dimensions depend on the time needed for the formation of new tungsten oxides at the bottom of the cavity. The larger size of the cavities associated with TiC particles is due to local microcracking, because oxygen transport must surround TiC coarse particles to arrive to the bottom of the cavity. The preferential oxidation attack into the metallic substrate is facilitated by the quick oxygen transport throughout the porous oxide scale, but there is certain oxide growth at the air/oxide interface, as noticed by the shifting of the outermost arrangements of cavities towards deeper locations in the scale; 3 and 10 μm for the materials oxidized 7 and 100 h at 600 ˚C, respectively. This oxide formation at the air/scale interface evidences the occurrence of some tungsten outward diffusion in the scale. Such transport can only occur if tungsten is transported outwards as a volatile oxide and, then, condensates as WO_3 at the outer surface as result of the increase in the oxygen partial pressure. Formation of observed nodules and their subsequent breakage to form craters will be the result of this process.

An interesting question is why the oxide scale formed on W-1TiC at 700 ˚C confers protection while the scale formed on pure tungsten is non-protective. Cross sectional views of the scale developed after 100 h at 700 ˚C reveals the absence of the multilayered scale consisting of

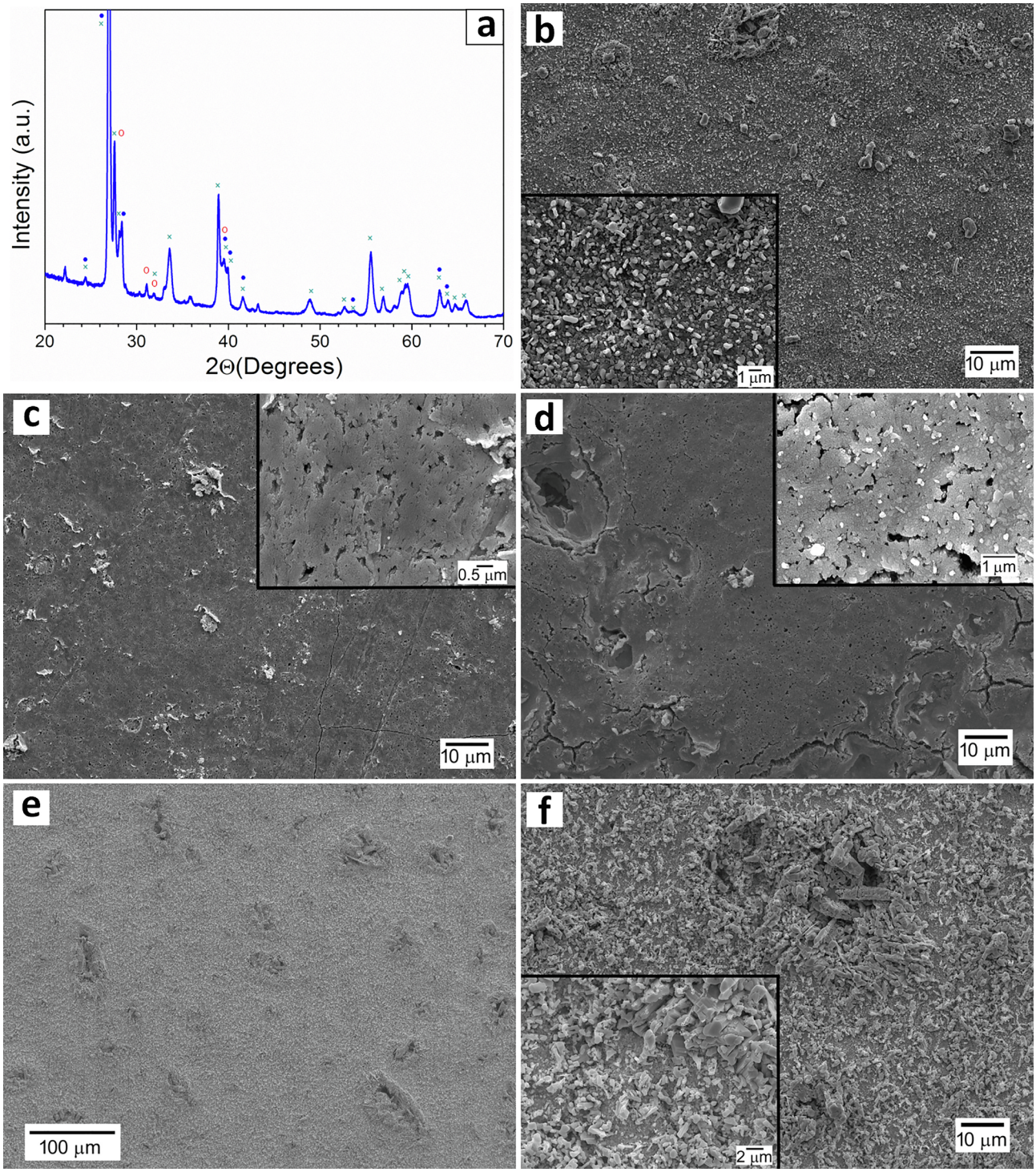

Fig. 4. (a) XRD pattern of W-1TiC oxidized in dry air for 100 h at 600 ˚C: × WO_3, ○ $W_{18}O_{49}$ and ● $WO_{2.92}$. The oxide scale formed on W-5TiC exhibits a similar diffraction pattern. SEM micrographs correspond to the surface of the scale formed at different temperatures and oxidation times. (b) W-1TiC after 100 h of oxidation in dry air at 600 ˚C (see the inset for a higher magnification). (c) & (d) W-5TiC after 1 h and 10 h of oxidation in dry air at 600 ˚C, respectively (see the inset for a higher magnification). (e) W-1TiC after 100 h of oxidation in dry air at 700 ˚C. Figure (f) corresponds to a higher magnification of this surface showing a crater and the predominant structure of the oxidized surface (see inset).

periodical arrangements of cavities found for pure tungsten. Instead, porosity randomly distributed over the entire thickness of the scale can be noticed. Only massive cracking in the central part of the scale is observed, which can be associated with the change from parabolic to linear kinetics observed in the mass gain curves. After a transient period, the scale becomes again denser, starting a new cycle of the oxidation process that results in a more protective scale. The effect of TiC should be related to prevent massive microcracking events occurring in pure tungsten. Microcracking is restricted to the locations in which TiC coarse particles are placed, preventing the periodical arrangements of cavities reported during the oxidation of pure tungsten at 700 ˚C.

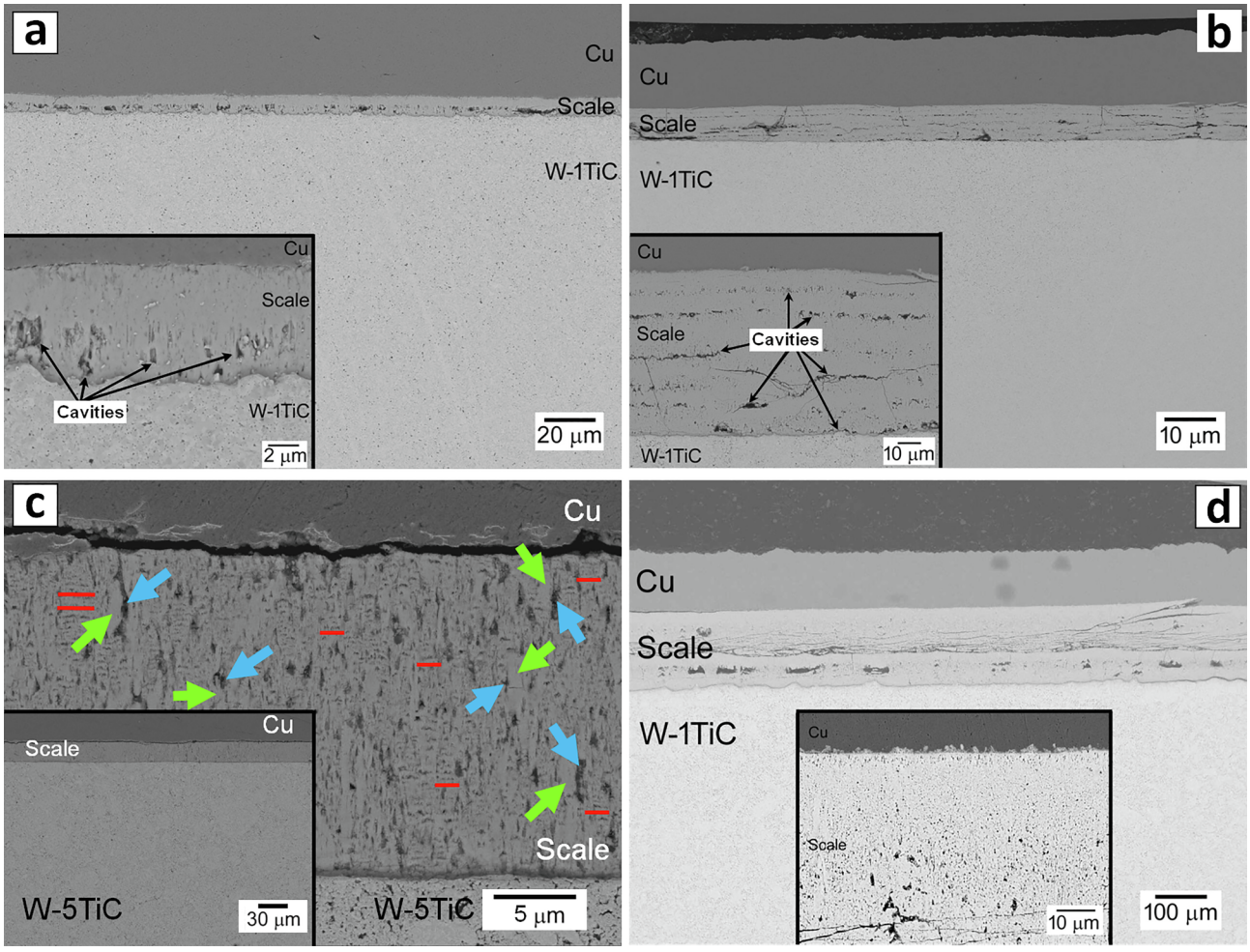

Fig. 5. Cross-section of the scale formed on the studied materials at different temperatures an exposure times. (a) & (b) W-1TiC oxidized for 7 h and 100 h in dry air at 600 °C, respectively. The insets show a detail at higher magnifications of the scale. (a) The arrows indicate some examples of large cavities formed within the scale. (b) The arrows mark the regions of the scale at which semicontinuous arrangements of cavities are generated during the oxidation process. (c) Cross-section of the scale formed on the W-5TiC oxidized for 1 h in dry air at 600 °C: red lines mark the semicontinuous bands of cavities, which are formed parallel to the original exposed surface, blue arrows indicate long cracks delimiting TiC-free and TiC-containing regions in the scale and green arrows denote dense regions of the oxide layer which coincide with TiC-free oxide. The inset depicts the scale at lower magnification. (d) W-1TiC oxidized for 100 h in dry air at 700 °C. The inset corresponds to a higher magnification of the outer part of the oxide scale.

5. Conclusions

From the present study the following conclusions can be drawn:

1. The influence of TiC addition on the oxidation behaviour of pure tungsten depends on the amount of TiC and the oxidation temperature. Low TiC additions and the presence of a lower density of coarse TiC particles, like that of W-1TiC, has a negligible effect on the oxidation behaviour of pure tungsten at 600 °C but reduces considerably the oxidation kinetics at 700 °C.
2. High TiC contents are always detrimental for the oxidation of pure tungsten. TiC coarse particles are formed and acts as stress concentrators, favouring microcracking events within the scale. In addition, TiC coarse particles promote decohesion among the TiC-free

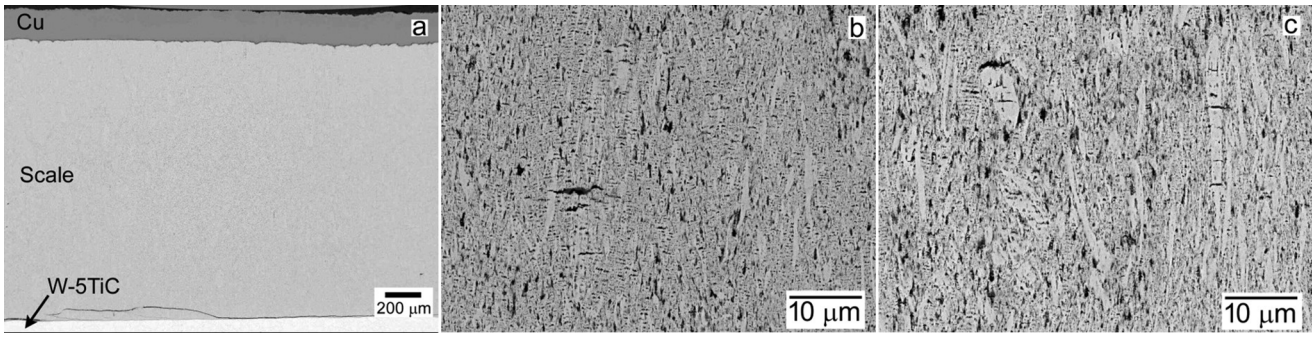

Fig. 6. Cross-section of the scale formed on the W-5TiC material oxidized for 100 h in dry air at 600 °C. (a) General view of the scale. (b) Detail of the outermost part of the scale. (c) Detail of the central part of the oxide scale.

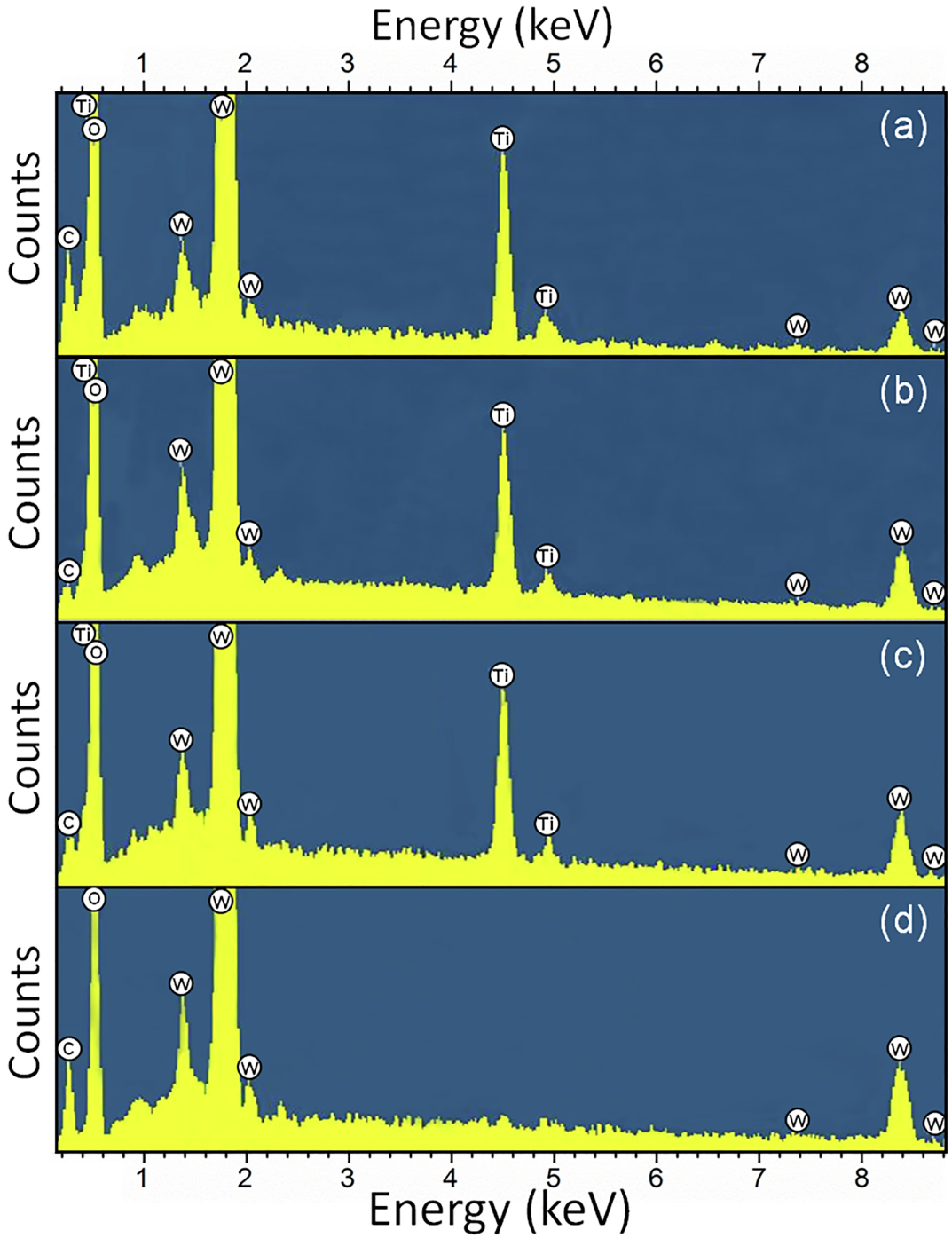

Fig. 7. Typical EDX spectra of particles inside cavities for W-1TiC oxidized for 7 h at 600 ˚C (a), W-1TiC oxidized for 7 h at 600 ˚C (b) and W-1TiC oxidized for 100 h at 700 ˚C (c). (d) EDX spectrum of the bulk oxide scale for W-1TiC oxidized 100 h at 700 ˚C.

and the TiC-containing regions existing in the metallic substrate.

3. Formation of cavities is associated with TiC coarse particles, so a higher content of TiC coarse particles leads to the formation of almost continuous cavities which facilitates inward oxygen transport into the metallic substrate, accelerating significantly the oxidation rate of the material.
4. When the mass fraction of TiC is low, as in the case of the W-1TiC alloy, TiC particles inhibit massive microcracking events occurring in pure tungsten in such a way that the oxide scale becomes denser because porosity/cavities are not connected. This beneficial effect is manifested during oxidation at 700 ˚C, leading to mass gain seven times lower than that found for pure tungsten.

CRediT authorship contribution statement

Pablo Pérez: Conceptualization, Methodology, Investigation, Writing - original draft, Visualization, Supervision, Funding acquisition. **Miguel A. Monge:** Conceptualization, Methodology, Investigation, Writing - review & editing, Supervision, Project administration, Funding acquisition. **Ángel Muñoz:** Methodology, Investigation, Formal analysis, Funding acquisition, Writing - review & editing. **Paloma Adeva:** Methodology, Investigation, Formal analysis, Writing - review & editing.

Declaration of Competing Interest

The authors declare that they have no known competing financial interests or personal relationships that could have appeared to influence the work reported in this paper.

Acknowledgments

This research has been supported by the Regional Government of Madrid through TECHNOFUSIÓN(III)CM (S2018/EMT-4437) and the Ministerio de Economía y Competitividad of Spain (ENE2015-70300-C3-2-R MINECO/FEDER) and programs. The authors acknowledge the expert support of A. García and A. Tomás from the CENIM Microscopy Laboratory.

References

[1] A. Loarte, Implications of the use of Carbon-Based Plasma Facing Components in Next Step Fusion Devices, Phys. Scr. T 111 (2004) 13–22, https://doi.org/10.1238/Physica.Topical.111a00013.
[2] R.A. Pitts, et al., Physics basis and design of the ITER plasma-facing components, J. Nucl. Mater. 415 (2011) S957–S964, https://doi.org/10.1016/j.jnucmat.2011.01.114.
[3] T. Hirai, et al., Use of tungsten material for the ITER divertor, Nucl. Mater. Energy 9 (2016) 616–622, https://doi.org/10.1016/j.nme.2016.07.003.
[4] T. Hirai, et al., Status of technology R&D for the ITER tungsten divertor monoblock, Nucl. Mater. 463 (2015) 1248–1251, https://doi.org/10.1016/j.jnucmat.2014.12.027.
[5] H. Bindslev (Director of Fusion for Energy) Annual Report 2013, Fusion For Energy. Fusion For Energy (2014). https://fusionforenergy.europa.eu/downloads/media-corner/publications/reports/ANNUAL_2013.pdf.
[6] R.G. Abernethy, Predicting the performance of tungsten in a fusion environment: a literature review, Mater. Sci. Tech. Ser. 33 (4) (2016) 388–399, https://doi.org/10.1080/02670836.2016.1185260.
[7] J.W. Coenen, et al., Plasma-wall interaction of advanced materials, Nucl. Mater. Energy 12 (2017) 307–312, https://doi.org/10.1016/j.nme.2016.10.008.
[8] A. Malizia, et al., A review of dangerous dust in fusion reactors: from its creation to its resuspension in case of LOCA and LOVA, Energies 9–578 (2016) 1–34, https://doi.org/10.3390/en9080578.
[9] D. Maisonnier, et al., DEMO and fusion power plant conceptual studies in Europe, Fusion Eng D 81 (2006) 1123–1130, https://doi.org/10.1016/j.fusengdes.2005.08.055.
[10] M. Rieth, et al., Recent progress in research on tungsten materials for nuclear fusion applications in Europe, J. Nucl. Mater. 432 (2013) 482–500, https://doi.org/10.1016/j.jnucmat.2012.08.018.
[11] A. Muñoz, et al., Microstructural and mechanical characteristics of W–2Ti and W–1TiC processed by hot isostatic pressing, J. Nucl. Mater. 455 (2014) 306–310, https://doi.org/10.1016/j.jnucmat.2014.06.064.
[12] A. Calvo, K. Schlueter, et al., Self-passivating tungsten alloys of the system W-Cr-Y for high temperature applications, Int. J. Refract. Met. Hard Mat. 73 (2018) 29–37, https://doi.org/10.1016/j.ijrmhm.2018.01.018.
[13] B. He, et al., Preparation and thermal shock characterization of yttrium doped tungsten-potassium alloy, J. Alloy. Compd. 86 (2016) 298–305, https://doi.org/10.1016/j.jallcom.2016.05.010.
[14] Y. Ishijima, H. Kurishita, Microstructure and Bend Ductility of W-0.3 mass%TiC Alloys Fabricated by Advanced Powder-Metallurgical Processing, Mater. Trans. 46 (2005) 568–574, https://doi.org/10.2320/matertrans.46.568.
[15] H. Kurishita, et al., Current status of ultra-fine grained W-TiC development for use in irradiation environments, Phys. Scr. T 128 (2007) 76–80, https://doi.org/10.1088/0031-8949/2007/T128/01.
[16] L. Dong-Guang, et al., An overview of oxidation-resistant tungsten alloys for nuclear fusion, J. Alloy. Compd. 765 (2018) 299–312, https://doi.org/10.1016/j.jallcom.2018.06.202.
[17] S.C. Cifuentes, M.A. Monge, P. Pérez, On the oxidation mechanism of pure tungsten in the temperature range 600–800 °C, Corrosion Sci. 57 (2012) 114–121, https://doi.org/10.1016/j.corsci.2011.12.027.
[18] C. Ma, D. Gu, D. Dai, H. Zhang, H. Zhang, J. Yang, M. Guo, Y. Du, J. Gao, Microstructure evolution and high-temperature oxidation behaviour of selective laser melted TiC/TiAl composites, Surf. Coat. Tech. 375 (2019) 534–543, https://doi.org/10.1016/j.surfcoat.2019.07.059.
[19] Y.-H. Lee, et al., Effect of TiC particle size on high temperature oxidation behavior of TiC reinforced stainless steel, App. Surf. Sci. 480 (2019) 951–955, https://doi.org/10.1016/j.apsusc.2019.02.138.
[20] E.A. Gulbransen, K.F. Andrew, Kinetics of the oxidation of pure tungsten from 500 degrees C to 1300 degrees C, J. Electrochem. Soc. 107 (1960) 619–628, https://doi.org/10.1149/1.2427787.